Volume 15
Number 16
21 August 2025
Pages 4601–4886

Catalysis Science & Technology

rsc.li/catalysis

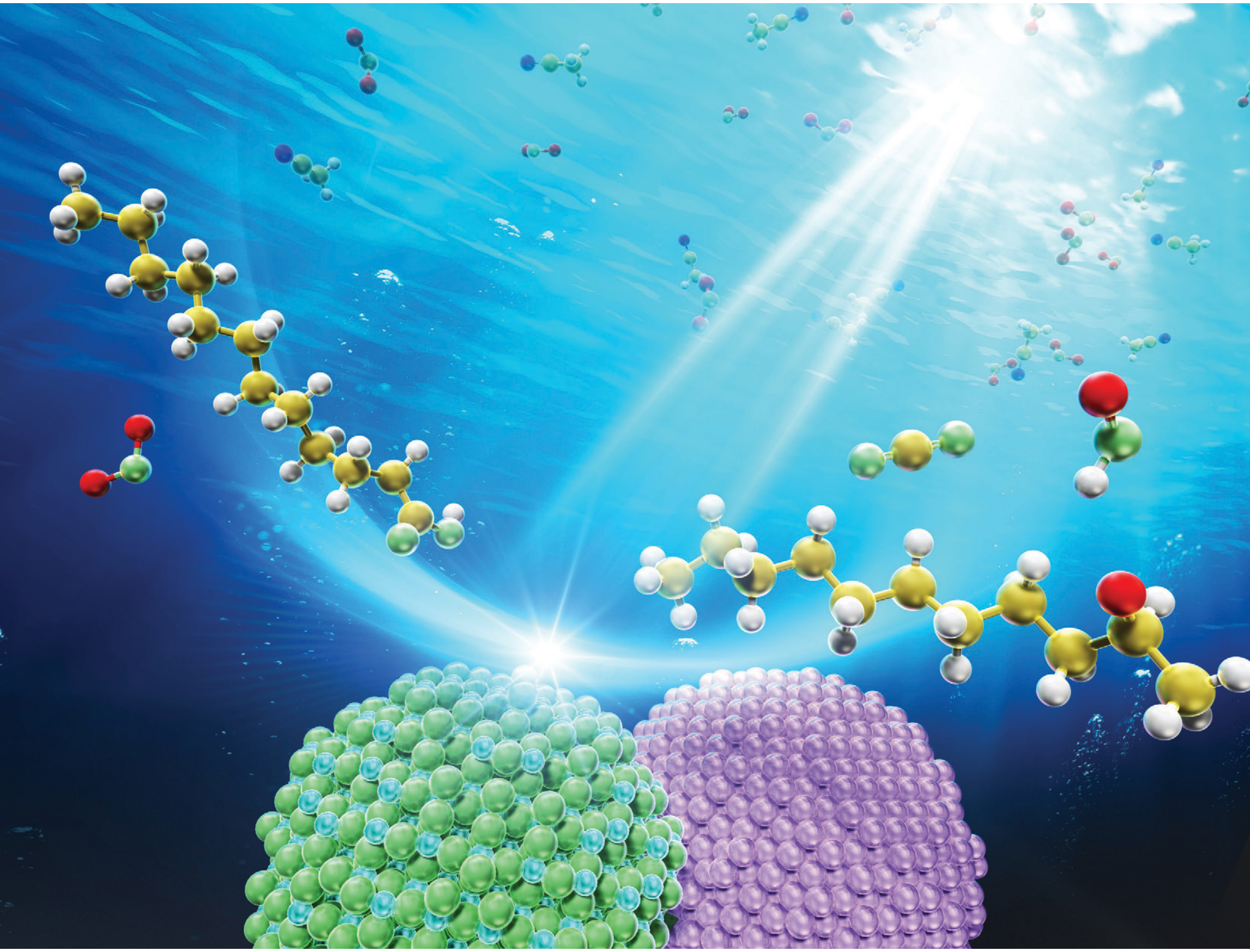

ISSN 2044-4761

ROYAL SOCIETY OF CHEMISTRY

PAPER
Hisao Yoshida *et al.*
Photocatalytic decarboxylative deuteration of lauric acid with heavy water for sustainable synthesis of deuterated alkanes

Catalysis Science & Technology

PAPER

Cite this: *Catal. Sci. Technol.*, 2025, **15**, 4637

Photocatalytic decarboxylative deuteration of lauric acid with heavy water for sustainable synthesis of deuterated alkanes†

Haifan Huang, [a] Zihan Lin,[a] Akira Yamamoto, [a] Yagna Bhoi Prakash, [a] Kexin Zou, [a] Shohichi Furukawa,[a] Ken-ichi Fujita, [a] Gunik Lee, [b] Jun Kumagai [c] and Hisao Yoshida *[a]

Received 14th March 2025,
Accepted 24th May 2025

DOI: 10.1039/d5cy00316d

rsc.li/catalysis

As a simple model system for sustainable synthesis of deuterated alkanes, photocatalytic decarboxylative deuteration of lauric acid (dodecanoic acid) was explored employing heavy water (^2H_2O, D_2O) as the deuterium source and titanium dioxide (TiO_2) photocatalysts loaded with metal cocatalysts (Au, Pt or Pd), without requiring any other reagents. The photocatalysts effectively facilitated the production of monodeuterated undecane ([$^2H_1$]undecane, $C_{11}H_{23}D$). The alkyl radical degenerated from lauric acid through decarboxylation couples with the deuterium radical generated from heavy water, resulting in the formation of the deuterated undecane. Among the tested photocatalysts, a gold-loaded TiO_2 (Au/TiO_2) photocatalyst pre-dried before use achieved a 15.3% yield of deuterated undecane after 3 hours of photocatalytic reaction, with the deuteration ratio (R_d) in the obtained undecane reaching 85.1%. While extending the reaction time increased the overall yield, it led to a lower R_d. The R_d did not reach 100% since the alkyl radical intermediate also reacts with lauric acid or another alkyl radical to form non-deuterated undecane ($C_{11}H_{24}$) or docosane ($C_{22}H_{46}$), respectively as byproducts. The reaction mechanism of this photocatalytic system was elucidated using ESR measurement with radical trapping. This study offers a model methodology for the efficient synthesis of deuterated compounds, with potential applications in various fields such as pharmaceuticals.

Introduction

Since the discovery of deuterium (^{2}H, or D), an isotope of hydrogen, in 1931,[1] deuterated compounds have played a crucial role in elucidating chemical reaction processes and mechanisms.[2,3] Deuterium is a cost-effective, safer, and more accessible labeling alternative compared to other isotopes[4] such as ^{13}C, ^{14}C, and ^{3}H. Additionally, the slower dissociation rate of the bond between deuterium and carbon provides distinct properties when compared to the typical hydrogen isotope (^{1}H). Recently, deuterium-labeled drugs have shown significant potential in drug development, as they are expected to extend the half-life of drug metabolism due to their slow reaction rate. For example, the first deuterated drug, Austedo (deuterated tetrabenazine), was approved by the US FDA in 2017 for the treatment of movement disorders.[5,6] Austedo is a modified form of tetrabenazine incorporating two deuterated methyl groups (including six deuterium atoms), which results in a drug with a prolonged life-time. Given these advancements, developing effective deuteration methods is of great significance in both pharmaceutical research and production.

In the past few years, considerable attention has been devoted to the development of new methods for the deuteration of organic molecules. Emerging techniques include reductive and deuterodehalogenation, photoredox-catalyzed labeling, and the development of transition metal catalytic systems.[7] Recently, some outstanding deuteration reactions have also been summarized in some review articles.[8–12]

Several primary methods for incorporating deuterium into an organic molecule include conventional multistep synthesis and direct hydrogen isotope exchange (HIE).[4,13,14] For instance, Kerr, *et al.*,[15] used D_2 as a deuterium source with homogeneous iridium catalysts to selectively deuterate indole, azaindole, and pyrrole N-heterocycles. Traditional HIE processes often require harsh conditions such as strong acids/bases,[16–20] flammable gases,[21–23] or multiple exchange processes[24–27] to ensure efficient deuterium incorporation. In addition, some cases

[a] *Graduate School of Human and Environmental Studies, Kyoto University, Yoshida-nihonmatsu-cho, Sakyo-ku, Kyoto 606-8501, Japan. E-mail: yoshida.hisao.2a@kyoto-u.ac.jp*
[b] *Department of Material Chemistry, Graduate School of Engineering, Nagoya University, Chikusa, Nagoya 464-8603, Japan*
[c] *Institute of Materials and Systems for Sustainability Division of Materials Research, Nagoya University, Furo-cho, Chikusa-ku, Nagoya, Aichi 464-8601, Japan*

† Electronic supplementary information (ESI) available. See DOI: **https://doi.org/10.1039/d5cy00316d**

involve costly deuterium sources.[28,29] Meanwhile, the precise and selective introduction of deuterium typically relies on functional groups like halogens, which can offer better position selectivity and efficiency than C–H/C–D exchange reactions. However, this approach still requires complex ligands and special deuterium donors like Et_3SiD[30] or Ph_2CDOH.[31] Furthermore, the large-scale applications of halogen-based methods raise environmental concerns. Therefore, there is a growing need for new, cost-effective, and environmentally friendly deuteration methodologies.

Photocatalytic synthesis has emerged as a promising approach for selective introduction of deuterium on organic molecules under mild conditions. Recent studies have reported photocatalytic dehalogenative deuteration of aryl halides using D_2O or CD_3CN as deuterium sources with photocatalysts such as Au/Cds,[13] CdSe,[32] and MOF.[33] However, these methods require the use of reducing reagents. Titanium oxide (TiO_2) photocatalyst, as a well-known semiconductor photocatalyst, can play a crucial role in the decomposition of organic pollutants,[34–38] water splitting,[39–44] and carbon dioxide reduction.[45,46] TiO_2 has also demonstrated promising photocatalytic performance in organic synthesis.[47–51] Kraeutler and Bard reported in 1978 that TiO_2 and platinated TiO_2 photocatalysts can produce methane (CH_4) and carbon dioxide (CO_2) primarily from acetic acid (CH_3COOH) aqueous solutions,[52,53] which is known as photo-Kolbe reaction (eqn (1)).

$$CH_3COOH \rightarrow CH_4 + CO_2 \tag{1}$$

In this reaction, the photocatalyst facilitates both the oxidation of acetic acid by holes, generating methyl radicals ($^{\bullet}CH_3$), CO_2, and protons (eqn (2)), and the reduction of protons by electrons to form hydrogen radicals ($H^{\bullet}$, eqn (3)). These radicals then couple to produce CH_4 (eqn (4)). Potential byproducts of this reaction include hydrogen and ethane, which are formed *via* radical homocoupling (eqn (5) and (6)).

$$CH_3COOH + h^+ \rightarrow {}^{\bullet}CH_3 + CO_2 + H^+ \tag{2}$$

$$H^+ + e^- \rightarrow H^{\bullet} \tag{3}$$

$${}^{\bullet}CH_3 + H^{\bullet} \rightarrow CH_4 \tag{4}$$

$$2H^{\bullet} \rightarrow H_2 \tag{5}$$

$$2{}^{\bullet}CH_3 \rightarrow C_2H_6 \tag{6}$$

Building on this reaction, our laboratory demonstrated a photocatalytic direct methylation of benzene under light irradiation using a platinum-loaded TiO_2 photocatalyst (Pt/TiO_2) with acetic acid as a methylation reagent.[54] This study suggests that the carboxyl group in organic acid (R–COOH) can serve as a possible leaving group, enabling the generation of corresponding alkyl radicals for the chemical reaction during photocatalytic decarboxylation. Organic acids, which commonly contain carboxyl groups, thus provide additional opportunities for deuterated substrates. In recent years, several studies have explored photocatalytic decarboxylative deuteration.[55–57] For example, Li *et al.*[55] achieved precise deuteration of aliphatic carboxylic acids by synergistic photoredox and HAT catalysis, obtaining good deuterium incorporation at predicted sites.

In this study, we explored a simple and sustainable reaction model system for photocatalytic decarboxylative deuteration, using lauric acid (LA) as the substrate and D_2O as the deuterium source to produce deuterated alkanes (eqn (7)). The reaction was conducted with a metal-loaded TiO_2 photocatalyst under light irradiation, without requiring any other reagents.

$$C_{11}H_{23}COOH + D_2O \rightarrow C_{11}H_{23}D + HDO + CO_2 \tag{7}$$

The successful production of the deuterated product was confirmed. In this reaction, alkyl radicals such as undecyl radical ($^{\bullet}C_{11}H_{23}$) and deuterium radical ($D^{\bullet}$) are formed from LA and heavy water prior to the formation of the deuterated undecane ($C_{11}H_{23}D$), denoted as C_{11}-*d* in the present study (eqn (8)–(10)) although non-deuterated undecane ($C_{11}H_{24}$, denoted as C_{11}-*h*) and docosane ($C_{22}H_{46}$, denoted as C_{22}) were also formed as dominant byproducts (eqn (11) and (12)).

$$C_{11}H_{23}COOH + h^+ \rightarrow {}^{\bullet}C_{11}H_{23} + CO_2 + H^+ \tag{8}$$

$$D^+ + e^- \rightarrow D^{\bullet} \tag{9}$$

$${}^{\bullet}C_{11}H_{23} + D^{\bullet} \rightarrow C_{11}H_{23}D\ (C_{11}\text{-}d) \tag{10}$$

$${}^{\bullet}C_{11}H_{23} + H^{\bullet} \rightarrow C_{11}H_{24}\ (C_{11}\text{-}h) \tag{11}$$

$$2{}^{\bullet}C_{11}H_{23} \rightarrow C_{22}H_{46}\ (C_{22}) \tag{12}$$

ESR spectroscopy provided insights into the possible reaction mechanism of this photocatalytic system. These findings demonstrate a straightforward, green, and cost-effective strategy for synthesizing deuterated compounds using organic acid and heavy water, including potential applications in the production of deuterated pharmaceuticals.

Results

Photocatalytic reaction tests with M/TiO_2 photocatalysts

The results of the photocatalytic reaction tests are summarized in Fig. 1A and Table S1.† After photoirradiation (wavelength > 360 nm) for 30 min, the target product, deuterated undecane (C_{11}-*d*), was obtained when TiO_2 or metal-loaded TiO_2 photocatalysts were used. The quantity of C_{11}-*d* contains one-deuterium undecane (C_{11}-d_1) and little doubly deuterated undecane (C_{11}-d_2, see Fig. S3†). In addition,

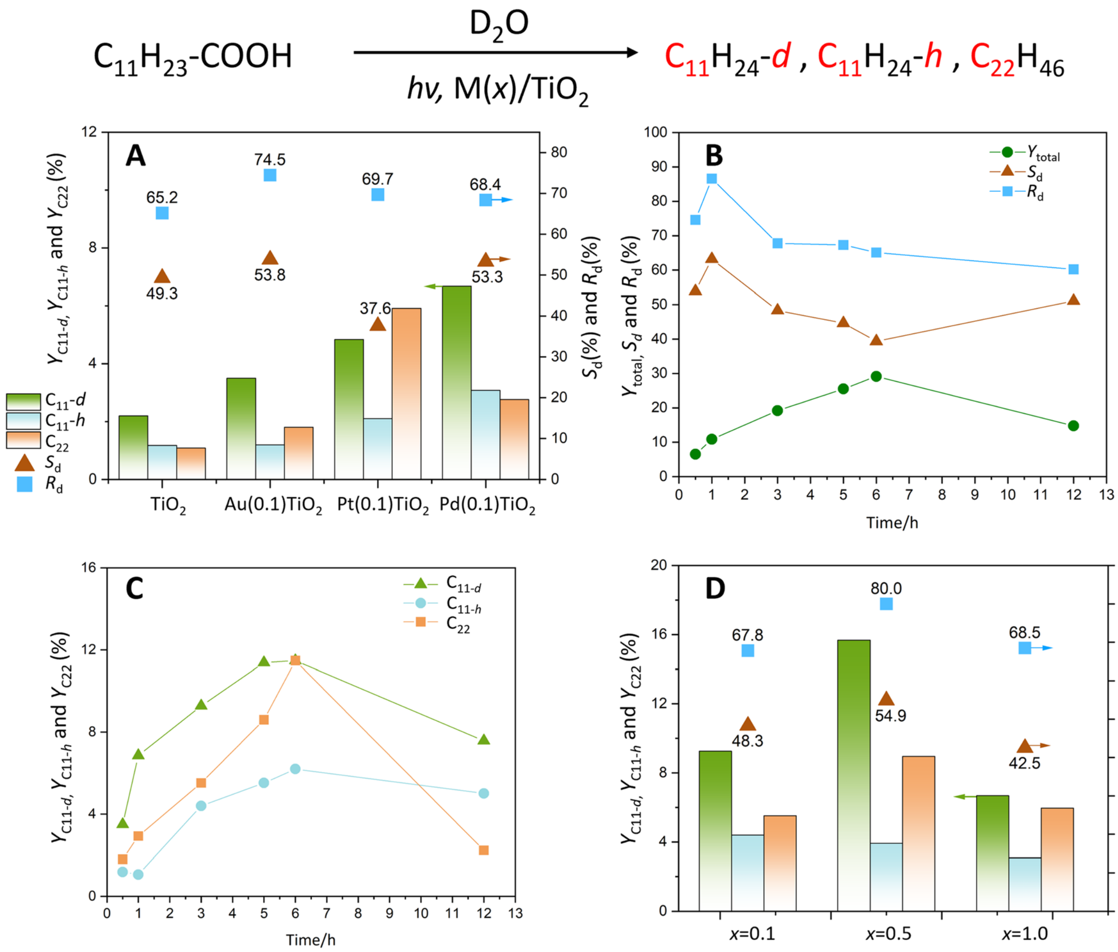

Fig. 1 Results of the reaction tests for photocatalytic decarboxylation of LA in the presence of heavy water: (A) results with the TiO_2 and $M(0.1)/TiO_2$ samples (M = Au, Pt, and Pd). The green, light blue, and orange bars represent. $Y_{C_{11}\text{-}d}$, $Y_{C_{11}\text{-}h}$, and $Y_{C_{22}}$, respectively. Dark red triangles indicate S_d (selectivity to C_{11}-*d*), and light blue squares show R_d (selectivity to C_{11}-*d* in the obtained undecanes). The reaction time was 0.5 h. Data are taken from Table S1;† see the caption of Table S1† for other reaction conditions. (B) Time course of Y_{total}, S_d, and R_d with the Au(0.1)/TiO_2 sample. (C) Time courses of $Y_{C_{11}\text{-}d}$, $Y_{C_{11}\text{-}h}$, and $Y_{C_{22}}$ with the Au(0.1)/TiO_2 catalysts. Detailed conditions for panels B and C are shown in Table S3.† (D) Results of the photocatalytic reaction tests with Au(*x*)/TiO_2 samples with different Au loading amounts (*x* wt%). The reaction time was 3 h. See also Table S4.†

non-deuterated undecane (C_{11}-*h*) and docosane (C_{22}) were detected as the dominant byproducts. Isomers of C_{22} were observed, though the amounts were very tiny. Further details can be found in the ESI.† Under certain conditions, oily products, likely resulting from successive polymerization, were observed. Regarding the gas-phase products, CO_2 and H_2 were detected; however, accurate quantitative analysis remained technically challenging.

Compared with the bare TiO_2 photocatalyst, the Au, Pt, and Pd metal-loaded TiO_2 samples exhibited higher photocatalytic activity for decarboxylation of LA as expected (Fig. 1A). Among the M(0.1)/TiO_2 photocatalysts, the Au(0.1)/TiO_2 sample gave lower total yield (Y_x) and C_{11}-*d* yield ($Y_{C_{11}\text{-}d}$) but higher selectivity toward C_{11}-*d* (S_d) compared to the Pt(0.1)/TiO_2 and Pd(0.1)/TiO_2 samples (Table S1†). The Pt(0.1)/TiO_2 sample showed the highest overall photocatalytic activity (Y_{total}) but the lowest selectivity to C_{11}-*d*, suggesting that the higher photocatalytic activity may lead to an increased concentration of alkyl radicals, promoting the formation of C_{22}, thus decreasing S_d value. This sample was employed for the mechanistic study as mentioned later. The Pd(0.1)/TiO_2 sample achieved the highest $Y_{C_{11}\text{-}d}$ (6.68%), though it exhibited a close value of S_d compared to Au(0.1)/TiO_2 sample due to the formation of a significant amount of by-products, C_{11}-*h* and C_{22}.

The selectivity of deuterated *n*-undecane (R_d), defined as the ratio of C_{11}-*d* to the total *n*-undecane (C_{11}-*d* and C_{11}-*h*) obtained, is a key parameter, as the separation of C_{11}-*d* from the mixture of undecane is very challenging. As shown in Fig. 1A, the Au(0.1)/TiO_2 sample exhibited the highest R_d. In contrast, the Pt(0.1)/TiO_2 and Pd(0.1)/TiO_2 samples showed comparatively lower R_d values. As discussed later, since R_d is determined by the reaction selectivity of the generated alkyl radical toward deuterium radical ($D^\bullet$) or other organic species, the highest R_d value is attributed to the properties of the Au cocatalyst. The reasons why the highest R_d did not reach 100% with any of the photocatalysts will be discussed later.

Results from blank reaction tests with the Au(0.5)/TiO_2 sample (Table S2†) indicated that both photoirradiation and the presence of a photocatalyst were essential for the reactions to occur, confirming that the deuteration proceeds photocatalytically. The time course study showed that the total yield of the products monotonously increased with time while the S_d and R_d decreased with time (Fig. 1B, Table S3†). The product distribution slightly varied with time (Fig. 1C, Table S3†). The $Y_{C_{11}\text{-}h}$ and $Y_{C_{22}}$ continuously increased, whereas the increase in the $Y_{C_{11}\text{-}d}$ slowed down with time. A possible explanation for this variation with time could be the change in the hydrophilic property of the photocatalyst surface due to the adsorption of hydrophobic products. Notably, the amount of main products decreased after 12 h of reaction, indicating that some successive reactions may happen to convert C_{11}-*d* into other products. Based on these results, the reaction time was set to 3 hours for all subsequent reaction tests. A recyclability test was also carried out, which led to a slight decrease in the C_{11}-*d* yield and R_d value. Details are described in the ESI,† Fig. S4. To improve the durability of the catalysts, improvements are required in the process of the catalyst recycling, catalyst surface modification, and improving the property of the loaded co-catalyst metals. By using a flow reactor, it might be possible to avoid these problems.[58]

Since the Au(0.1)/TiO_2 sample showed the best R_d value among the three M(0.1)/TiO_2 samples (Fig. 1A), additional Au(x)/TiO_2 samples were tested with varying Au loading, and the results were presented in Fig. 1D and Table S4.† The Au(0.5)/TiO_2 sample demonstrated the best performance, achieving a high $Y_{C_{11}\text{-}d}$ (15.7%) and a high R_d (80%) under these conditions. It is observed that the Au(1.0)/TiO_2 sample exhibited lower activity compared to the Au(0.5)/TiO_2 sample, as shown in Fig. 1D and Table S4.† This decline in performance at higher loadings may be attributed to the aggregation of Au nanoparticles (NPs), which is known to occur when the metal content exceeds a certain threshold. At higher metal loadings, the particle size of metal NPs tends to increase, leading to a

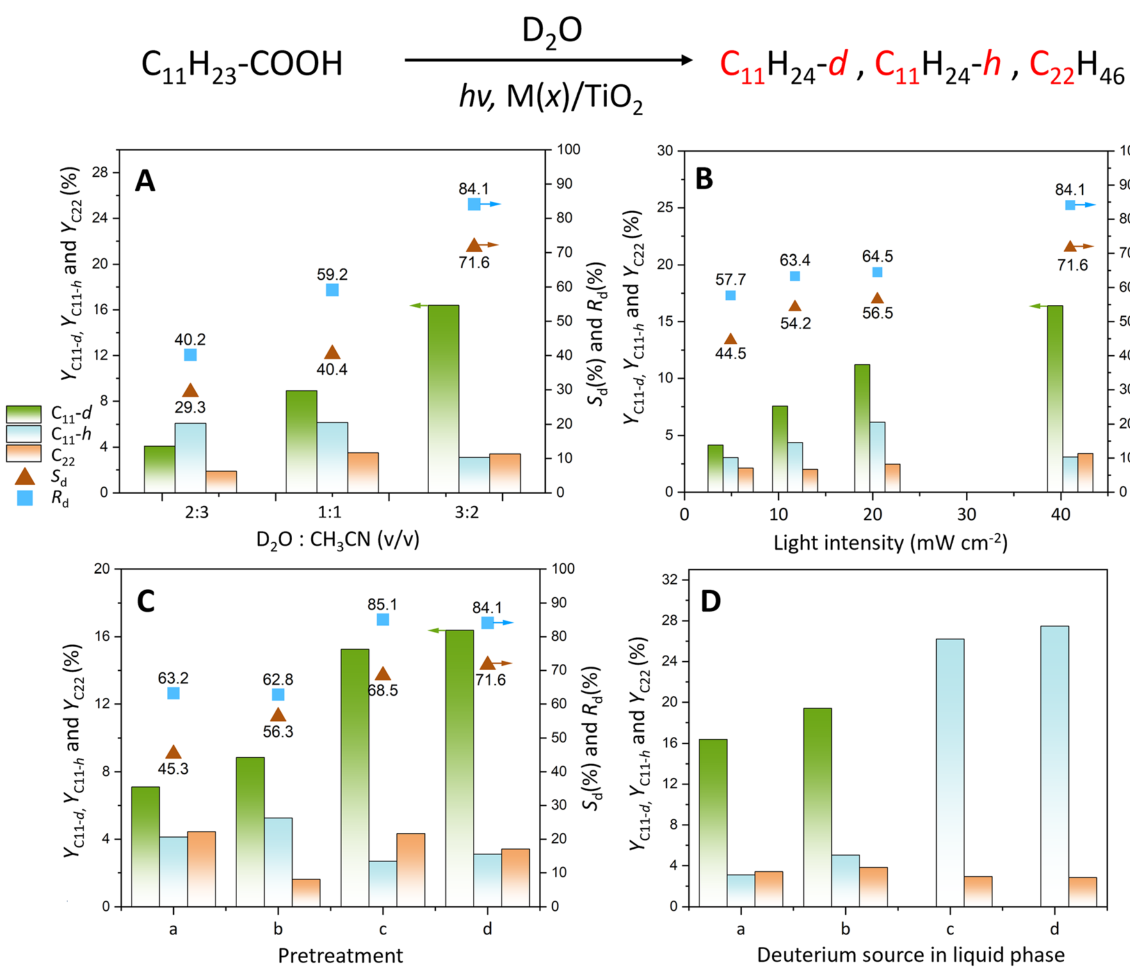

Fig. 2 Results of photocatalytic reaction tests with the Au(0.5)/TiO_2 sample. (A) Different ratios of D_2O and CH_3CN. (B) Dependence on light intensity. (C) Various pre-treatments, (a) without any pre-treatment, (b) with pre-irradiation in the presence of D_2O, (c) with pre-heating and pre-irradiation in the presence of D_2O, and (d) with pre-heating and pre-irradiation in the absence of D_2O as a standard condition. (D) Various liquid phases: (a) D_2O/CH_3CN, (b) D_2O/CD_3CN, (c) H_2O/CD_3CN, and (d) H_2O/CH_3CN. Other reaction conditions for panels A, B, C and D are provided in the captions of Tables S5–S8,† respectively.

reduced surface area. This decrease in surface area may, in turn, lower the efficiency of electron transfer required for the reduction, thus decreasing the overall photocatalytic activity. This phenomenon has been reported in similar systems and highlights the importance of optimizing metal dispersion for maintaining catalytic efficiency.[59–61]

Mechanistic studies

As mentioned above, the R_d could not reach 100% with any of the photocatalysts under these conditions. This suggests that hydrogen (^{1}H) from other compounds or materials reacted with the photocatalytically generated undecyl radical (eqn (11)). To increase the R_d and to elucidate the reaction mechanism, additional experiments were conducted as described below.

Reaction conditions. First, three different ratios of D_2O and CH_3CN ($D_2O:CH_3CN$ = 2:3, 1:1, 3:2. v/v) were examined (Fig. 2A). To maintain a constant total reactant volume of 5 mL, 2 mL, 2.5 mL, and 3 mL of D_2O were used, corresponding to 40, 50, 60% of total. Higher D_2O proportions resulted in better $Y_{C_{11}\text{-}d}$ and higher R_d values. However, since LA does not fully dissolve in solutions with higher concentrations of D_2O, experiments using more than 3 mL of D_2O were not conducted in the present study. From these results, a high concentration of D_2O is beneficial for producing deuterated compounds.

Subsequently, the photocatalytic reaction was carried out at varying light intensities (Fig. 2B). The $Y_{C_{11}\text{-}d}$ increased with light intensity, while $Y_{C_{11}\text{-}h}$ initially increased until the intensity reached 21 mW cm^{-2}, after which it decreased at a higher light intensity. In contrast, $Y_{C_{22}}$ remained relatively stable across different light intensities. These results suggest that the production of C_{11}-*d* is enhanced by light intensity, while the radical coupling process that produces C_{22} is not significantly influenced by light intensity. At higher light intensities, more alkyl radicals are utilized to form C_{11}-*d* rather than C_{11}-*h*. In addition, R_d increased as the light intensity was increased, and further discussion of this trend can be found in the succeeding section.

Pretreatment. To determine whether initial impurities such as adsorbed organic matter, water (^1H_2O), or hydroxy groups on the surface of the photocatalyst sample could serve as hydrogen (^{1}H) sources or not, we examined alternative pre-treatments. These included pre-heating and pre-irradiation, replacing the typical pre-treatment prior to photocatalytic reaction tests. Pre-heating was intended to remove adsorbed organic matter and water, while pre-irradiation was aimed at facilitating H/D exchange of surface hydroxy groups on the photocatalyst before the photocatalytic reaction test.

The results are shown in Fig. 2C and Table S7.† Although pre-irradiation without pre-heating enhanced the photocatalytic activity and selectivity for deuterated undecane (S_d), it did not improve R_d (Fig. 2Cb). In contrast, pre-heating led to higher $Y_{C_{11}\text{-}d}$ and an improved R_d, with values of 15.3% and 85.1%, respectively (Fig. 2Cb and Cc). Heating the sample in an argon flow at 450 K effectively should remove adsorbed organic matter and water, reducing the formation of C_{11}-*h* and enhancing R_d. Furthermore, when pre-heating was performed, pre-irradiation (with or without D_2O) did not significantly impact R_d (Fig. 2Cc and Cd). The best result with the highest R_d (85.1%) among them was achieved under the conditions shown in Fig. 2Cc. These findings highlight that removing initially adsorbed impurities on the photocatalyst surface improves R_d, although complete R_d remains still unachieved.

Deuterium sources. Next, we tested the photoreaction using deuterated acetonitrile (CD_3CN) instead of CH_3CN since the solvent was also a candidate of the hydrogen source. Fig. 2D depicts a set of control experiments conducted in different solvents (CH_3CN and CD_3CN) and water (D_2O and H_2O) using the Au(0.5)/TiO_2 photocatalyst (see also Table S8†). The $Y_{C_{11}\text{-}d}$ was not improved by using CD_3CN as a solvent (Fig. 2Dd), which confirmed that the solvent in this protocol is irrelevant to the synthesis of deuterated alkane. At the same time, it was proved that D_2O serves as the only deuterium source in this system, which is the same as the results in literature: for instance, in the case of the CdSe photocatalyst used for dehalogenative deuteration of aryl halides in D_2O/CH_3CN, D_2O activation occurs to offer deuterium radicals ($D^\bullet$) to promote the reaction.[13,32]

When H_2O was used, no deuterated alkane was detected regardless of the isotopic property of acetonitrile (Fig. 2Dc and Dd), confirming that D_2O is the sole deuteration source. In addition, it was observed that the $Y_{C_{11}\text{-}h}$ was higher than the combined yields of $Y_{C_{11}\text{-}d}$ and $Y_{C_{11}\text{-}h}$ obtained with D_2O (Fig. 2Da and Db). This result indicates an isotopic effect. Considering that the C_{11}-*h* obtained in the presence of D_2O (Fig. 2Da) is produced *via* the reaction of an alkyl radical with an organic compound, the $Y_{C_{11}\text{-}h}$ in the absence of D_2O (Fig. 2Dd) should include C_{11}-*h* formed in the same way. Thus, the k_H/k_D value for C_{11} production with H_2O or D_2O can be estimated to be 1.58. Similarly, the amount of C_{22} obtained was higher, further supporting an isotopic effect with a k_H/k_D of 1.74. These findings suggest that the reaction rate is slower when breaking the D–OD bond in D_2O (eqn (13) and (14)) compared to the H–OH bond in H_2O, indicating that the activation of D_2O to form either radical species (eqn (13) or (14)) is the rate-determining steps (RDS) in this reaction system. However, the separate study revealed that the formation of $^\bullet$OD radical (eqn (14)) would be minor due to the presence of LA.[62] Thus, the observed RDS would be the water reduction (eqn (13)). The plausible pathways for LA oxidation by the $^\bullet$OD radical are likely minor (eqn (15) and (16)).

$$D_2O + e^- \rightarrow D^\bullet + OD^- \tag{13}$$

$$D_2O + h^+ \rightarrow {}^\bullet OD + D^+ \text{ (minor)} \tag{14}$$

$$C_{11}H_{23}COOH + {}^\bullet OD \rightarrow {}^\bullet C_{11}H_{23} + CO_2 + HDO \text{ (minor)} \tag{15}$$

$$C_{11}H_{23}COOH + {}^\bullet OD \rightarrow {}^\bullet C_{11}H_{22}COOH + HDO \text{ (minor)} \tag{16}$$

As mentioned, the R_d did not reach 100% even under the optimized conditions. This suggests that another hydrogen (^1H) source contributing to the formation of C_{11}-*h* should still exist within the reaction system. Remaining possible hydrogen sources are the organic molecules, such as LA and the produced undecane. It is proposed that the undecyl radical, photocatalytically generated from LA, could react with another LA (eqn (17)) or the produced alkanes (eqn (18)). The former will give deuterated or non-deuterated LA and the latter can give doubly deuterated undecane ($C_{11}H_{22}D_2$).

$$^{\bullet}C_{11}H_{23} + C_{11}H_{23}COOH \rightarrow C_{11}H_{24}\ (C_{11}\text{-}h) + {}^{\bullet}C_{11}H_{22}COOH \quad (17)$$

$$^{\bullet}C_{11}H_{23} + C_{11}H_{23}D \rightarrow C_{11}H_{24}\ (C_{11}\text{-}h) + {}^{\bullet}C_{11}H_{22}D \quad (18)$$

In addition, one may consider that protons (H^+) formed from LA (eqn (8)) would be reduced by photoexcited electrons, potentially contributing to the generation of C_{11}-*h* and thus decreasing the R_d. However, it cannot be ignored that the amount of LA (50 μmol) is limited, whereas D_2O (56 mmol) is in excess. The dissociated protons from LA react with the excess D_2O to form deuterated hydronium ions (D_2HO^+), which can subsequently release D^+ instead of H^+, as shown in eqn (19). This suggests that protons (H^+) dissociated from LA are unlikely to be reduced by photoexcited electrons to generate H· radicals, and therefore contribute negligibly to the formation of C_{11}-*h*. Therefore, the pathway shown in eqn (20) highly a minor contributor to the overall product formation.

$$H^+ + D_2O \rightarrow HDO + D^+ \quad (19)$$

$$^{\bullet}C_{11}H_{23} + H^{\bullet} \rightarrow C_{11}H_{24}\ (C_{11}\text{-}h)\ (\text{minor route}) \quad (20)$$

Therefore, achieving complete selectivity to deuterated alkane would be difficult when using these kinds of organic acids like LA. To further increase the R_d value, the reaction rate of radical coupling between the alkyl radical and deuterium radical (eqn (10)) should be improved by further optimization of reaction conditions and improvement in photocatalyst properties.

Position of deuterium in the product. Considering that the photo-Kolbe reaction of acetic acid proceeds *via* decarboxylation to form methyl radical, one may expect that a linear carboxylic acid would generate a primary alkyl radical, which is an alkyl radical with the radical center at the terminal carbon originally bonded to the carboxy group. In the case of LA, this would initially form an undecyl radical, with the radical center at the terminal carbon, $^{\bullet}CH_2(CH_2)_9CH_3$. On the other hand, quantum chemical calculations using Gaussian 16 (Table S9†)[63] showed that the secondary radical having the radical center at the second carbon from the terminal one, $CH_3^{\bullet}CH(CH_2)_8CH_3$, is the most stable among the alkyl radicals.

Radical intermediate species photocatalytically generated from LA were detected by using ESR measurement with a radical trapping method. A spin trapping reagent, DBNBS, trapped the radical species generated from LA with the Pt(0.1)/TiO_2 photocatalyst and formed some kinds of radical adducts. The spectrum is shown together with the calculated spectra in Fig. 3. Simulation of the obtained ESR spectra revealed that the spectrum consisted of two components: the major one (93.8%) was an adduct trapping secondary radical, while the minor one (6.2%) was the adduct trapping primary radical. In our previous work,[62] ESI-MS analysis clarified the presence of two major secondary radicals formed from LA: one of these radicals was a secondary alkyl radical, represented as $CH_3(CH_2)_x^{\bullet}CH(CH_2)_{8-x}CH_3$ (x = 0–4), and another contained a carboxy group, represented as $CH_3(CH_2)_x^{\bullet}CH(CH_2)_{9-x}COOH$ ($0 \le x \le 9$). These facts evidenced that the primary and the secondary alkyl radicals generated from LA were present under the presence conditions. When the radical species containing a carboxy group reacts with a deuterium radical ($D^{\bullet}$), it forms deuterated LA, meaning that it does not directly contribute to the formation of deuterated undecane in the initial stage. On the other hand, the primary and the secondary alkyl radicals can serve as the reaction intermediates, possibly forming the corresponding deuterated undecane.

Among the possible secondary alkyl radicals, the one with the radical center at the second carbon from the terminal ($CH_3^{\bullet}CH(CH_2)_8CH_3$) would be the most stable radical as mentioned above (Table S9†). Since the primary radical initially generated from LA is thermodynamically unfavorable, radical rearrangement reaction likely occurs. This rearrangement involves an intramolecular hydrogen atom transfer, which converts the primary radical into a more stable secondary radical with the radical center at the second carbon from the terminal (eqn (21)).

$$\begin{aligned}&^{\bullet}CH_2(CH_2)_9CH_3\ (\text{primary alkyl radical})\\ &\rightarrow CH_3{}^{\bullet}CH(CH_2)_8CH_3\ (\text{secondary alkyl radical})\end{aligned} \quad (21)$$

Therefore, the major deuterated undecane (C_{11}-*d*) obtained in the present system would be 2-deuterated *n*-undecane with deuterium incorporated at the second carbon from the terminal, $CH_3CHD(CH_2)_8CH_3$ (eqn (22)). This selectivity is determined thermodynamically. The 1-deuterated *n*-undecane would be the minor C_{11}-*d* product (eqn (23)).

$$CH_3{}^{\bullet}CH(CH_2)_8CH_3 + D^{\bullet} \rightarrow CH_3CHD(CH_2)_8CH_3 \quad (22)$$

$$^{\bullet}CH_2(CH_2)_9CH_3 + D^{\bullet} \rightarrow CH_3(CH_2)_9CH_2D \quad (23)$$

On the other hand, the main isomer of docosane (C_{22}) obtained was *n*-docosane, which should be formed *via* the radical–radical coupling of the primary undecyl radical (Scheme S2a†). This could be explained by the difference in the reaction rate, including the migration rate. Two

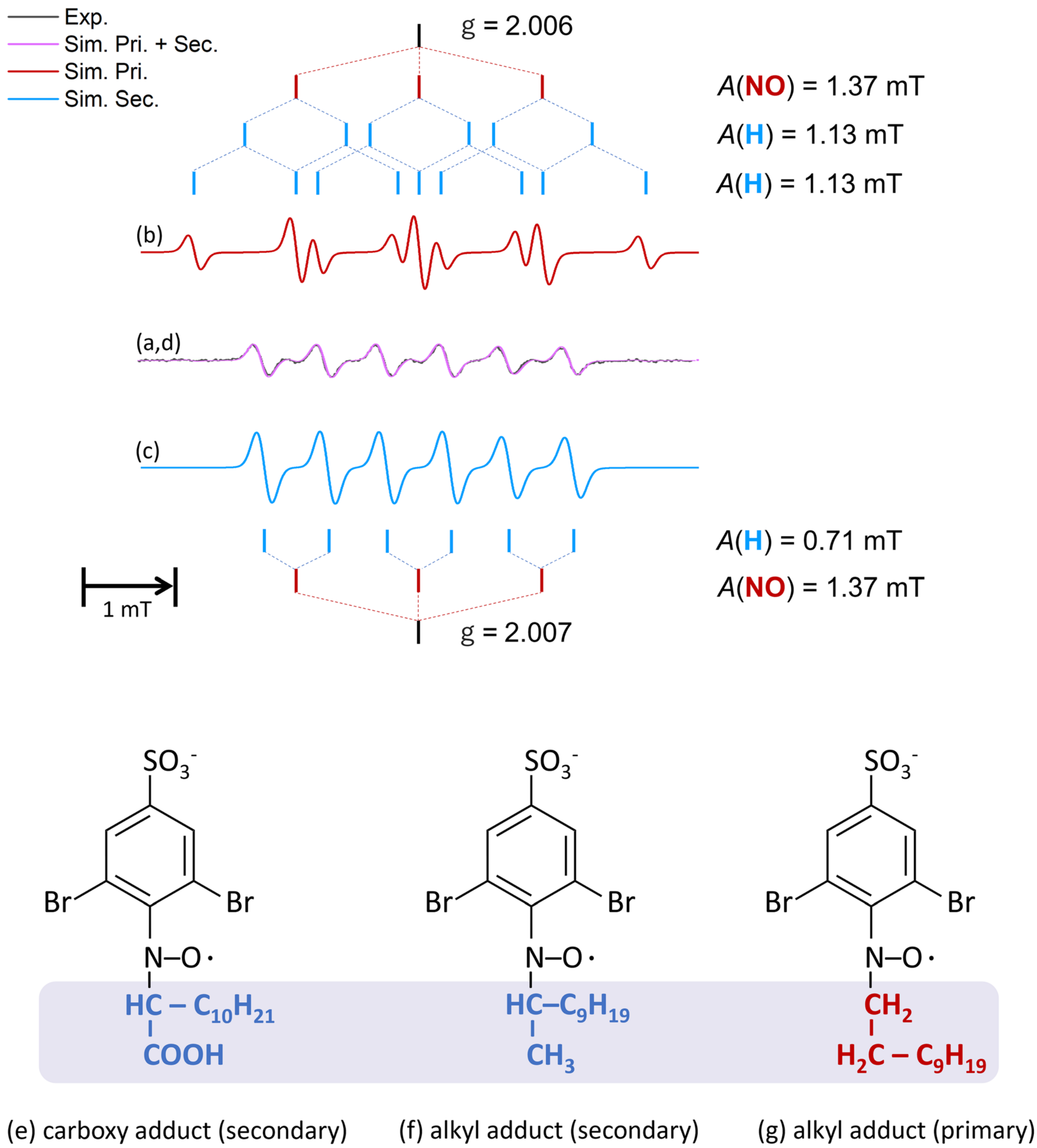

Fig. 3 Observed ESR spectrum of DBNBS-adduct-trapping radical species in supernatants of the resulting mixture after the photocatalytic reaction (a, black), and calculated spectra of primary radicals (b, red), secondary radicals (c, blue) and the sum of simulated spectra (d, overlapped to the observed spectrum), along with the representative spin adduct structures of carboxy secondary radical (e), alky secondary radical (f), and alkyl primary radical (g). The photocatalytic reaction was carried out in a mixed solvent of water (0.6 mL) and acetonitrile (0.4 mL), containing 10 mM of lauric acid ($C_{11}H_{23}COOH$), 10 mM of DBNBS, and 10 mg of the Pt(0.1)/TiO_2 photocatalyst. The simulation parameters for hyperfine coupling constants are A_{NO} = 1.37 mT, A_H = 1.13 mT for the primary radical; A_{NO} = 1.37 mT, A_H = 0.71 mT for the secondary radicals, respectively.

primary undecyl radicals initially produced *via* decarboxylation at the oxidation sites on the TiO_2 photocatalyst can immediately combine prior to the intramolecular hydrogen atom transfer (eqn (21)). On the other hand, the rate of crosscoupling between the undecyl radical and deuterium radical ($D^•$) including the mass transfer rate would be relatively slow so that the intramolecular hydrogen atom transfer (eqn (21)) would occur before the crosscoupling of the radicals, producing $CH_3CHD(CH_2)_8CH_3$ (eqn (22)).

Proposed reaction mechanisms

Formation of deuterated undecane. Based on the results mentioned above, we propose a mechanism for the decarboxylation reaction of LA in the presence of D_2O leading to the formation of deuterated undecane (C_{11}-d_1) predominantly $CH_3CHD(CH_2)_8CH_3$ (Scheme 1). This mechanism is a one-photon radical process.

Upon photoirradiation, the TiO_2 photocatalyst generates electron–hole pairs. In the presence of a metal cocatalyst, the generated charge carries are spatially separated to

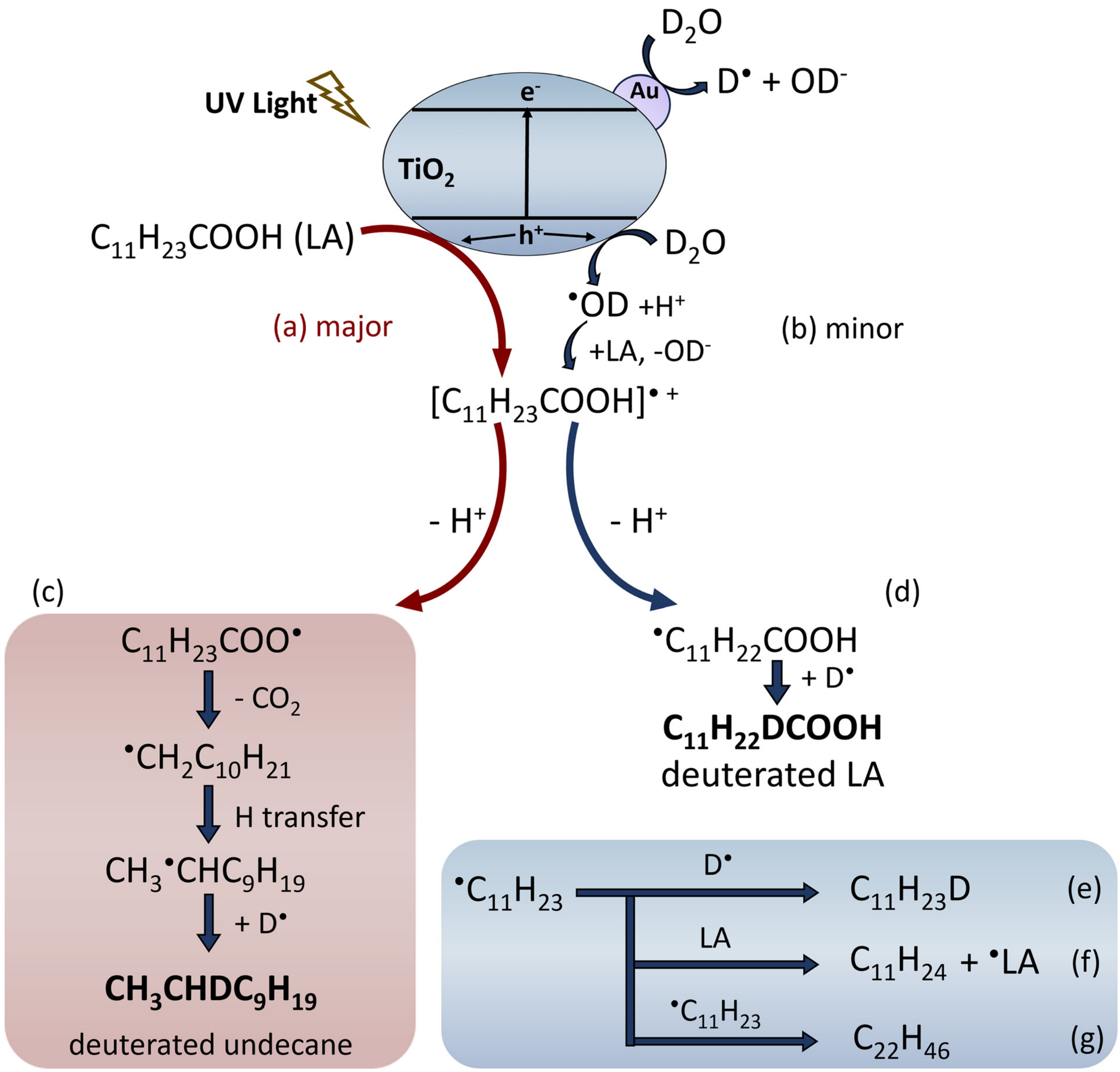

Scheme 1 Proposed mechanism for the production of deuterated undecane in the photocatalytically decarboxylation of LA in the presence of D_2O; formation of LA radical cation intermediates through (a) the direct hole oxidation or (b) indirect oxidation facilitated by $^\bullet$OD radical, and successive alternative reactions of the LA radical cation for (c) the production of deuterated undecane and (d) the production of deuterated lauric acid, the latter of which does not directly produce deuterated undecane, and (e–g) three reaction pathways of alkyl radical.

some extent, with the electrons migrating to the cocatalyst and the holes reaching the TiO_2 surface. A molecule of LA ($C_{11}H_{23}COOH$) adsorbed on the TiO_2 surface is oxidized by a photogenerated hole, resulting in the formation of an unstable LA cation radical, $[C_{11}H_{23}COOH]^{+\bullet}$ (Scheme 1a). Alternative minor oxidation process is mediated by OD radical ($^\bullet$OD) to form the LA cation radical (Scheme 1b). On the other hand, D_2O is reduced to deuterium radicals ($D^\bullet$) and OD^- by photoexcited electrons on the metal cocatalyst (eqn (15)), which is suggested by the observation of isotope effect. This generation of hydroxy anions through reduction is balanced by the formation of protons *via* oxidation mentioned below.

The cation radical subsequently releases a proton (H^+), leading to the formation of either a carboxyl radical, $[C_{11}H_{23}COO]^\bullet$ (Scheme 1c) or an LA radical, $^\bullet C_{11}H_{22}COOH$ (Scheme 1d). Among the two routes, the former directly generates a molecular CO_2 and an undecyl radical, $^\bullet C_{11}H_{23}$, where the initially produced primary undecyl radical, $^\bullet CH_2(CH_2)_9CH_3$, changes to the secondary radical, $CH_3^\bullet CH(CH_2)_8CH_3$ as a result of intramolecular hydrogen transfer prior to the final radical coupling step due to its higher thermodynamic stability as discussed above. Combining with deuterium radical, the target deuterated *n*-undecane featuring deuterium substitution at the second carbon from the terminal carbon, $CH_3CHD(CH_2)_8CH_3$ is formed (Scheme 1c). This is the major product C_{11}-*d* in this system. The latter, the LA radical, does not directly contribute to the undecane formation (Scheme 1d).

Three reaction pathways of alkyl radicals ($^{\bullet}C_{11}H_{23}$) are summarized in Scheme 1e–g. Only when the formed alkyl radical reacts with $^{\bullet}$D (or D_2O), the deuterated alkane is formed (Scheme 1e). On the other hand, when it reacts with LA or alkyl radical, byproducts (C_{11}-*h* or C_{22}, respectively) are formed. To improve the R_d value, suppressing pathway f and increasing the pathway e are options worth considering. Furthermore, increasing the proportion of D_2O in the system or improving the hydrophilicity of the catalyst surface are both possible effective methods to enhance the R_d. Additionally, reducing the occurrence of pathway g is also beneficial for improving S_d.

Side reactions. Here, the side reactions are discussed. On the reduction sites, molecular hydrogen (it should be predominantly D_2) was also formed from homocoupling of two hydrogen radicals (mainly $D^{\bullet}$) as shown in eqn (5). The Pt cocatalyst is well known as a good catalyst for the hydrogen radical coupling compared to the Au cocatalyst,[64] which would be one of the reasons for the lower R_d value of the Pt/TiO_2 photocatalyst. The exact reason why the Au cocatalyst gave the higher R_d remains unclear. However, it is believed that its effectiveness lies in its ability to suppress such side reactions other than deuteration.

The undecyl radicals possibly react with some other chemical species, such as lauric acid, undecane, $H^{\bullet}$ radical, to form the undecane-*h* (eqn (21), (22) and (25)) and with undecyl radical to give docosane (Scheme S2†), which reduced the R_d value down to 85% even in the best conditions in the present study. Like we discussed in the previous section, because of the large amount of D_2O and small amount of LA, the H^+ or H radicals formed from LA are exposed to a large amount of heavy water and they are unlikely to be involved in the reaction. Therefore, the main reason for the incomplete selectivity, S_d and R_d are the reaction of the undecyl radical with other organic matters in the reaction system, such as LA, undecane, and undecyl radical.

Additionally, when the alkyl carboxylic radical ($^{\bullet}C_{11}H_{22}COOH$) combines with a deuterium radical ($D^{\bullet}$) in route B, deuterated LA is formed. This may give doubly deuterated undecane ($C_{11}H_{22}D_2$), the presence of which was suggested by the GC-MS analysis (see Fig. S3†). Although C_{11}-d_2 compounds were usually formed only in trace amounts, under the conditions where their formation was particularly pronounced, they accounted for up to 30% of the total C_{11}-*d* compounds. This result confirms that the formation of deuterated LA molecule ($C_{11}H_{22}DCOOH$), which provides further support for the proposed Scheme 1(d). The formation of C_{11}-*h* is attributed to the reaction between alkyl radicals and LA molecule.

Light intensity. Based on the above mechanism, we propose an explanation for the increase in R_d with higher light intensity. First, the number of photogenerated electrons and holes increases as light intensity increases. On the oxidation side, the increase in holes promotes the formation of alkyl radicals, while on the reduction side, the increase in electrons enhances the production of $D^{\bullet}$ radicals as mentioned above. The reaction between the increased numbers of alkyl radicals and $D^{\bullet}$ radicals results in the formation of more deuterated alkanes in the system. In contrast, the reaction of alkyl radicals with LA produces non-deuterated alkane, but the amount of LA does not increase with light intensity. Consequently, high light intensity preferentially leads to the production of deuterated alkane over non-deuterated alkane, thereby increasing the R_d.

Experimental

Catalyst preparation

All metal-loaded titanium oxide (M/TiO_2) photocatalysts were prepared by a photodeposition method with a commercial TiO_2 sample (Ishihara Sangyo Kaisha, ST-01, anatase, 300 $m^2\ g^{-1}$). Aqueous solutions of metal precursors, $HAuCl_4$ (Nacalai Tesque, 99%), H_2PtCl_6 (Nacalai Tesque, 99%), and $PdCl_2$ (Kishida Chemical, 99%), were used at concentrations of 9.89, 7.53, and 6.37 g L^{-1} as Au, Pt, and Pd, respectively.

The preparation of the Au(0.5)/TiO_2 sample is described as a representative example as follows. First, 2.0 g of TiO_2 powder was dispersed in 300 mL of ion-exchanged water and irradiated with a xenon lamp (PE300BUV, 300 W) for 30 min under magnetic stirring. Subsequently, 100 mL of methanol and 1 mL of the $HAuCl_4$ solution (9.894 g L^{-1} as Au) were added to the suspension. The mixture was stirred for 15 min without irradiation, followed by stirring for 1 h under light irradiation. After irradiation, the suspension was filtered and washed with over 500 mL of deionized water. The wet residue was dried in an electric oven at 353 K for 12 h, yielding a purple-colored powder of the Au(0.5)/TiO_2 sample. Here, x in M(x)/TiO_2 represents the metal loading amount as weight percent (wt%).

Other M(x)/TiO_2 photocatalysts were synthesized using similar procedures.

Synthesis of monodeuterated *n*-undecane with Grignard reagent

The *n*-[1-$^2H_1$]undecane ($CH_3(CH_2)_9CH_2D$) as a reference was synthesized by the Grignard reagent (see ESI,† Scheme S1).

Photocatalytic reaction tests

The photocatalytic reaction test was conducted in a closed system using a capped 20 mL quartz tube. Typically, 50 mg of the photocatalyst was introduced and subjected to pre-heating at 450 K using a metal bath for 30 min in an argon gas flow (15 ml min^{-1}) to remove adsorbed water. Then the catalyst underwent pre-irradiation with a xenon lamp (PE300BUV, 300 W) for 15 min to clean the catalyst surface. Following the pre-heating and pre-irradiation, 5 mL of reactant solution containing LA (50 μmol), D_2O (3 mL), and acetonitrile (CH_3CN, 2 mL) was added to the quartz tube. The tube was sealed with a white silicone septum stopper and Parafilm, the air was purged from the tube using an argon flow (15 ml min^{-1}) for 30 min, and the contents were stirred under light irradiation for the desired duration (typically, 180 min) using an optical filter that permitted light with wavelengths >360 nm to promote the photocatalytic reaction. The reaction is carried out at an ambient temperature of 25 °C.

Optimization experiments were conducted under various conditions, including reaction time (Fig. 1), D_2O concentration, light intensity, pretreatment conditions, and deuterium source (Fig. 2).

After the reaction, the liquid phase was filtered through a syringe equipped with a PTFE membrane filter and analyzed qualitatively and quantitatively using gas chromatography with GC-MS (Shimadzu QP-2020) and GC-FID (Shimadzu GC-2014), with *n*-decane ($C_{10}H_{22}$) as an internal standard. Details of the analysis for deuterated products and byproducts are described in the ESI.† The gas-phase products were detected by GC-TCD prior to the liquid-phase analysis.

The yield of product, Y_x (%) (x = C_{11}-*d*, C_{11}-*h*), $Y_{C_{22}}$ (%), the selectivity to deuterated undecane, S_d (%), and the ratio of deuterated undecane in the obtained undecane, R_d, were defined as follows (eqn (24)–(27)):

$$Y_x\,(\%) = 100 \times A_x/A_{\text{initial LA}} \tag{24}$$

$$Y_{C_{22}}\,(\%) = 100 \times 2 \times A_{C_{22}}/A_{\text{initial LA}} \tag{25}$$

$$S_d\,(\%) = 100 \times A_{C_{11}\text{-}d}/(A_{C_{11}\text{-}d} + A_{C_{11}\text{-}h} + 2 \times A_{C_{22}}) \tag{26}$$

$$R_d\,(\%) = 100 \times A_{C_{11}\text{-}d}/(A_{C_{11}\text{-}d} + A_{C_{11}\text{-}h}) \tag{27}$$

where A_x shows the amount of substance x. Specifically, $A_{\text{initial LA}}$ is the amount of initially introduced LA (50 μmol), $A_{C_{11}\text{-}d}$ and $A_{C_{11}\text{-}h}$ correspond to the amounts of [$^2H_1$]undecane ($C_{11}H_{23}D$, referred to as C_{11}-*d*) and undeuterated undecane ($C_{11}H_{24}$, referred to as C_{11}-*h*), respectively. GC-MS analysis also suggested the formation of a tiny amount of [$^2H_2$] undecane, referred to as C_{11}-d_2, which was included in $A_{C_{11}\text{-}d}$. The amounts of docosane (*n*-docosane, $C_{22}H_{46}$, referred to as C_{22}) were referred to $A_{C_{22}}$. Due to technical difficulties in the direct quantitative analysis of LA, total yield, Y_{total} (%) was used as an index of photocatalytic activity, which corresponds to the amount of the produced undecyl radical and defined as follows (eqn (28)).

$$Y_{\text{total}}\,(\%) = 100 \times (A_{C_{11}\text{-}d} + A_{C_{11}\text{-}h} + 2 \times A_{C_{22}})/A_{\text{initial LA}} \tag{28}$$

Analyses of radical intermediates

Electron spin resonance (ESR) spectra of spin adducts were recorded at room temperature by a JES-RE1X spectrometer (JEOL Co. Ltd, Japan) equipped with a TE102 cavity using a quartz flat cell as described.[62] The Pt(0.1)/TiO_2 photocatalyst powder (10 mg) was put into a disposable test tube (D-10S, Nichiden-Rika Glass Co., Ltd., 75 mm height, o.d. = 10 nm, i.d = 8 mm) and pre-irradiated with a high-pressure Hg lamp (Ushio UI-501C) for 30 min to purify the catalyst surface. After the pre-irradiation, a reaction mixture of ultrapure water (H_2O, 0.6 mL), acetonitrile (CH_3CN, 0.4 mL), and LA (10 mM) were added to the test tube. Subsequently, 0.01 mM of DBNBS (3,5-dibromo-4-nitrosobenzenesulfonate sodium salt ($C_6H_2NO_4SBr_2Na$), Kyoto Spin Lab, ≥95%) was introduced as a spin-trapping reagent. The sample was then irradiated through an optical filter (wavelength ≥350 nm) for 10 min. Following the photoirradiation, the mixture was centrifuged at 1.0 × 10^4 rpm for 5 min, and the supernatant was used for ESR measurement. Manganese (Mn^{2+}) dispersed in magnesium oxide (JEOL, Co. Ltd., Japan) served as the reference for sensitivity and *g*-value calibration. The ESR spectra of DBNBS spin adducts were simulated using EasySpin 6.0.0 software on MATLAB®, employing the "garlic" core function without additional perturbations.

Conclusions

In this study, we successfully demonstrated a simple and sustainable method for the synthesis of deuterated alkanes using lauric acid ($C_{11}H_{23}COOH$) as an example. Metal-loaded TiO_2 photocatalysts facilitate photocatalytic decarboxylation of carboxylic acid, followed by successive deuteration using heavy water (D_2O), yielding deuterated alkane (deuterated undecane, $C_{11}H_{23}D$, C_{11}-*d*). Compared with the limited C_{11}-*d* yield and deuteration selectivity achieved with the bare TiO_2 sample, the Au(0.5)/TiO_2 photocatalyst sample showed a significantly improved performance, achieving a high yield ($Y_{C_{11}\text{-}d}$ = 15.3%) and a deuterated undecane ratio in the obtained undecane (R_d = 85.1%) in the present best conditions (Fig. 2Cc).

$C_{11}H_{23}COOH$ molecule adsorbed on the TiO_2 surface is oxidized by a photogenerated hole, resulting in a LA cation radical, which subsequently generates an undecyl radical, $^{\bullet}C_{11}H_{23}$. Combining with a deuterium radical, the target deuterated *n*-undecane is formed.

The major product was identified as deuterated *n*-undecane with deuterium substitution predominantly occurring at the second carbon from the terminal carbon, $CH_3CDH(CH_2)_8CH_3$. Mechanistic investigations suggested that the limited selectivity arose from undesirable side reactions of the radical intermediate with other organic species, including the substrate, the derived radical species, and products. Further investigation to overcome these points is still desired.

These findings highlight a valuable strategy for synthesizing deuterated compounds by using heavy water (D_2O) as the deuterium source, providing a pathway for simple and highly selective deuteration reactions with broad potential applications.

Data availability

The authors confirm that the data supporting the findings of this study are available within the manuscript and its ESI.† Raw data that support the findings of this study are available from the corresponding author, upon reasonable request.

Author contributions

HH: investigation, methodology, and writing – original draft; ZL: investigation and methodology; AY: investigation and funding acquisition; BYP, KZ, SF, KF, GL and JK: investigation; HY: conceptualization, supervision, writing – review & editing, and funding acquisition.

Conflicts of interest

There are no conflicts to declare.

Acknowledgements

The authors acknowledge Prof. Naoki Komatsu of Kyoto University for his kind discussion. This study was financially supported by the Grant-in-Aid for Scientific Research (A) (22H00274) and the Grant-in-Aid for the Promotion of Joint International Research (Fostering Joint International Research (B), 20KK0116) from the Japan Society for the Promotion of Science (JSPS).

References

1 H. Kragh, *Stud. Hist. Philos. Sci. B: Stud. Hist. Philos. Mod. Phys.*, 2012, **43**, 176–183.
2 C. S. Elmore, *Annu. Rep. Med. Chem.*, 2009, **44**, 515–534.
3 Y. Y. Loh, K. Nagao, A. J. Hoover, D. Hesk, N. R. Rivera, S. L. Colletti, I. W. Davies and D. W. C. Macmillan, *Science*, 2017, **358**, 1182–1187.
4 W. Ou, C. Qiu and C. Su, *Chin. J. Catal.*, 2022, **43**, 956–970.
5 S. H. DeWitt and B. E. Maryanoff, *Biochemistry*, 2018, **57**, 472–473.
6 C. Scnmidt, *Nat. Biotechnol.*, 2017, **35**, 493–495.
7 S. Kopf, F. Bourriquen, W. Li, H. Neumann, K. Junge and M. Beller, *Chem. Rev.*, 2022, **122**, 6634–6718.
8 H. Li, M. Shabbir, W. Li and A. Lei, *Chin. J. Chem.*, 2024, **42**, 1145–1156.
9 G. Prakash, N. Paul, G. A. Oliver, D. B. Werz and D. Maiti, *Chem. Soc. Rev.*, 2022, **51**, 3123–3163.
10 N. Li, Y. Li, X. Wu, C. Zhu and J. Xie, *Chem. Soc. Rev.*, 2022, **51**, 6291–6306.
11 P. L. Norcott, *Chem. Commun.*, 2022, **58**, 2944–2953.
12 R. Zhou, L. Ma, X. Yang and J. Cao, *Org. Chem. Front.*, 2021, **8**, 426–444.
13 Y. Dong, Y. Su, L. Du, R. Wang, L. Zhang, D. Zhao and W. Xie, *ACS Nano*, 2019, **13**, 10754–10760.
14 A. Di Giuseppe, R. Castarlenas and L. A. Oro, *C. R. Chim.*, 2015, **18**, 713–741.
15 W. J. Kerr, D. M. Lindsay, P. K. Owens, M. Reid, T. Tuttle and S. Campos, *ACS Catal.*, 2017, **7**, 7182–7186.
16 P. Ranjan, S. Pillitteri, E. V. Van Der Eycken and U. K. Sharma, *Green Chem.*, 2020, **22**, 7725–7736.
17 J. Atzrodt, V. Derdau, T. Fey and J. Zimmermann, *Angew. Chem., Int. Ed.*, 2007, **46**, 7744–7765.
18 Y. Chang, A. Yesilcimen, M. Cao, Y. Zhang, B. Zhang, J. Z. Chan and M. Wasa, *J. Am. Chem. Soc.*, 2019, **141**, 14570–14575.
19 A. Martins and M. Lautens, *Org. Lett.*, 2008, **10**, 4351–4353.
20 F. Bourriquen, N. Rockstroh, S. Bartling, K. Junge and M. Beller, *Angew. Chem., Int. Ed.*, 2022, **61**, e202202423.
21 T. Kurita, K. Hattori, S. Seki, T. Mizumoto, F. Aoki, Y. Yamada, K. Ikawa, T. Maegawa, Y. Monguchi and H. Sajiki, *Chem. – Eur. J.*, 2008, **14**, 664–673.
22 W. N. Palmer and P. J. Chirik, *ACS Catal.*, 2017, **7**, 5674–5678.
23 V. Pfeifer, T. Zeltner, C. Fackler, A. Kraemer, J. Thoma, A. Zeller and R. Kiesling, *Angew. Chem., Int. Ed.*, 2021, **60**, 26671–26676.
24 Z. Yu, W. Wang and L. Chen, *J. Labelled Compd. Radiopharm.*, 2011, **54**, 352–356.
25 C. Zhang, Z. Shen, L. Tian and L. Chen, *J. Labelled Compd. Radiopharm.*, 2012, **55**, 401–405.
26 M. Fang and K. R. Cadwallader, *J. Agric. Food Chem.*, 2013, **61**, 3580–3588.
27 G. Srinivas, V. K. P. Unny, K. Mukkanti and B. M. Choudary, *J. Labelled Compd. Radiopharm.*, 2013, **56**, 325–329.
28 J. Atzrodt, V. Derdau, W. J. Kerr and M. Reid, *Angew. Chem., Int. Ed.*, 2018, **57**, 3022–3047.
29 J. Martin, J. Eyselein, S. Grams and S. Harder, *ACS Catal.*, 2020, **10**, 7792–7799.
30 C. S. Donald, T. A. Moss, G. M. Noonan, B. Roberts and E. C. Durham, *Tetrahedron Lett.*, 2014, **55**, 3305–3307.
31 M. Kuriyama, N. Hamaguchi, G. Yano, K. Tsukuda, K. Sato and O. Onomura, *J. Org. Chem.*, 2016, **81**, 8934–8946.
32 C. Liu, Z. Chen, C. Su, X. Zhao, Q. Gao, G. H. Ning, H. Zhu, W. Tang, K. Leng, W. Fu, B. Tian, X. Peng, J. Li, Q. H. Xu, W. Zhou and K. P. Loh, *Nat. Commun.*, 2018, **9**, 80.
33 T. Luo, Z. Wang, Y. Chen, H. Li, M. Peng, F. Tuna, E. J. L. McInnes, S. J. Day, J. An, M. Schröder and S. Yang, *Angew. Chem., Int. Ed.*, 2023, **62**, e202306267.
34 C. S. Turchi and D. F. Ollis, *J. Catal.*, 1990, **122**, 178–192.
35 T. Yang, J. Peng, Y. Zheng, X. He, Y. Hou, L. Wu and X. Fu, *Appl. Catal., B*, 2018, **221**, 223–234.
36 L. B. Reuterglrdh and M. Langphasuk, *Chemosphere*, 1997, **35**, 585–596.
37 Y. Sari, P. L. Gareso, B. Armynah and D. Tahir, *Int. J. Hydrogen Energy*, 2024, **55**, 984–996.
38 A. Fujishima, T. N. Rao and D. A. Tryk, *J. Photochem. Photobiol., C*, 2000, **1**, 1–21.
39 M. Ni, M. K. H. Leung, D. Y. C. Leung and K. Sumathy, *Renewable Sustainable Energy Rev.*, 2007, **11**, 401–425.
40 J. C. Smart, B. L. Pinsky, M. F. Fredrich and V. W. Day, *J. Am. Chem. Soc.*, 1979, **101**, 4373–4374.
41 K. Yamaguti and S. Sato, *J. Chem. Soc., Faraday Trans. 1*, 1985, **81**, 1237–1246.
42 T. Kawai and T. Sakata, *Chem. Phys. Lett.*, 1980, **72**, 87–89.
43 S. Sato and J. M. White, *Chem. Phys. Lett.*, 1980, **72**, 83–86.
44 H. Eidsvåg, S. Bentouba and P. Vajeeston, *et al.*, *Molecules*, 2021, **26**, 1687.
45 H. Abdullah, M. M. R. Khan, H. R. Ong and Z. Yaakob, *J. CO_2 Util.*, 2017, **22**, 15–32.
46 A. Hammad, A. Anzai, X. Zhu, A. Yamamoto, D. Ootsuki, T. Yoshida, A. EL-Shazly, M. Elkady and H. Yoshida, *Catal. Lett.*, 2020, **150**, 1081–1088.

47 H. Yuzawa and H. Yoshida, *Chem. Lett.*, 2013, **42**, 1336–1343.
48 D. Friedmann, A. Hakki, H. Kim, W. Choi and D. Bahnemann, *Green Chem.*, 2016, **18**, 5391–5411.
49 S. Kohtani, E. Yoshioka, K. Saito, A. Kudo and H. Miyabe, *Catal. Commun.*, 2010, **11**, 1049–1053.
50 K. Imamura, T. Yoshikawa, K. Hashimoto and H. Kominami, *Appl. Catal., B*, 2013, **134–135**, 193–197.
51 N. Hoffmann, *Aust. J. Chem.*, 2015, **68**, 1621–1639.
52 B. Kraeutler and A. J. Bard, *J. Am. Chem. Soc.*, 1978, **100**, 2239–2240.
53 B. Kraeutler and A. J. Bard, *J. Am. Chem. Soc.*, 1978, **100**, 5985–5992.
54 K. Zou, A. Yamamoto and H. Yoshida, *Catal. Today*, 2024, **425**, 114354.
55 N. Li, Y. Ning, X. Wu, J. Xie, W. Li and C. Zhu, *Chem. Sci.*, 2021, **12**, 5505–5510.
56 Y. He, H. Yang, D. Gao, J. Ma, Y. Shao, G. An and G. Li, *Chin. J. Org. Chem.*, 2021, **41**, 4725–4731.
57 Z. Huang, Z. Zhao, C. Zhang, J. Lu, H. Liu, N. Luo, J. Zhang and F. Wang, *Nat. Catal.*, 2020, **3**, 170–178.
58 H. Yoshida, *Adv. Energy Sustainability Res.*, 2025, 2400439.
59 S. Park, J. Jeong, K. I. Fujita, A. Yamamoto and H. Yoshida, *J. Am. Chem. Soc.*, 2020, **142**, 12708–12714.
60 H. Yuzawa, M. Aoki, K. Otake, T. Hattori, H. Itoh and H. Yoshida, *J. Phys. Chem. C*, 2012, **116**, 25376–25387.
61 H. Yuzawa, J. Kumagai and H. Yoshida, *J. Phys. Chem. C*, 2013, **117**, 11047–11058.
62 G. Lee, R. Maruyama, K. Zou, H. Huang, K. Oyama, H. Yoshida and J. Kumagai, *J. Phys. Chem. C*, 2025, **129**, 402–414.
63 M. J. Frisch, G. W. Trucks, H. B. Schlegel, G. E. Scuseria, M. A. Robb, J. R. Cheeseman, G. Scalmani, V. Barone, G. A. Petersson and H. Nakatsuji, *et al.*, *Gaussian 16*, Vers. Revision C.02, Gaussian, Inc., Wallingford CT, 2019.
64 K. Zou, A. Yamamoto and H. Yoshida, *Int. J. Hydrogen Energy*, 2024, **91**, 989–996.

